World Journal of Advanced Research and Reviews
eISSN: 2581-9615 CODEN (USA): WJARAI
Cross Ref DOI: 10.30574/wjarr
Journal homepage: https://wjarr.com/

(RESEARCH ARTICLE)

Check for updates

Comparative analysis of deep neural network and artificial neural network for predicting wheat water content using UAV multispectral and thermal imagers

Adama Traore [1], Mahamadou Konare [2], Syed Tahir Ata-Ul-Karim [3], Sunusi Amin Abubakar [5], Seydou Traore [4], Aiwang Duan [5] and Ben Zhao [5,*]

[1] *Laboratoire Société Mobilité Environnement, Département de Sociologie, Université Joseph KI-ZERBO (UJKZ), Ouagadougou, Burkina Faso.*
[2] *Laboratoire Sciences et Technologie (LaST), Unité de Formation et de Recherche en Sciences et Technique (UFR ST), Université Thomas SANKARA (UTS), 12 BP 417 Ouagadougou 12, Burkina Faso.*
[3] *Graduate School of Agricultural and Life Sciences, The University of Tokyo, 1-1-1 Yayoi, Bunkyo, Tokyo 113-8657, Japan*
[4] *Metropolitan Solar Inc., Washington, DC 20032, USA.*
[5] *Key Laboratory of Crop Water Use and Regulation, Ministry of Agriculture, Farmland Irrigation Research Institute, Chinese Academy of Agricultural Sciences, 380 Hongli road, Xinxiang Henan 453003, P.R. China.*

World Journal of Advanced Research and Reviews, 2024, 24(02), 058–072

Publication history: Received on 17 September 2024; revised on 27 October 2024; accepted on 30 October 2024

Article DOI: https://doi.org/10.30574/wjarr.2024.24.2.3281

Abstract

Water is a vital component for the growth of wheat and the quality of its grains. The measurement of plant water content (PWC) serves as a crucial indicator for assessing the water status of crops, thereby guiding effective irrigation management practices. Recent advancements in technology, particularly the use of multispectral and thermal imaging from unmanned aerial vehicles (UAVs), offer the capability to capture a comprehensive view of PWC variability across agricultural fields. This study aimed to create predictive models for PWC utilizing artificial neural networks (ANN), deep neural networks (DNN), and traditional stepwise regression techniques, all based on the analysis of multispectral and thermal imagery. To effectively evaluate the water content in wheat, we combined high-resolution thermal and multispectral imaging techniques with machine learning approaches. This assessment was carried out through three distinct experiments, which included one conducted in a rainout shelter and two performed under rainfed conditions. The findings demonstrated that UAV-derived multispectral imagery, when coupled with machine learning models, can effectively predict wheat plant water content with remarkable precision. Notably by considering all the dataset, DNN model exhibited superior performance (R2=0.96, ENS=0.98, RMSE=1.37%, MAE=0.98%) compared to both the ANN (R2=0.95, ENS=0.95, RMSE=1.88%, MAE=1.46%,) and the stepwise regression model (SRM) (R2=0.67, ENS=0.51, RMSE=10.79%, MAE=9.03%). Across all machine learning approaches, both the DNN and ANN models significantly outperformed the stepwise regression model in predictive accuracy. The statistical outcomes derived from the calibration phase indicate that both the trained Artificial Neural Networks (ANN) and Deep Neural Networks (DNN) serve as effective instruments for accurate prediction of PWC. Notably, the DNN network demonstrates superior accuracy compared to ANN.

Keywords: Machine learning; Deep neural network; UAV sensors; Plant water content

1. Introduction

Water is an essential element of wheat growth and grain quality and plays a crucial role in their photosynthetic activities, which are essential for achieving optimal agricultural yields. Given its importance in the vegetative cycle of crops, particularly wheat, water stress can have detrimental effects on both growth and productivity. Numerous studies

* Corresponding author: Ben Zhao

have highlighted various negative impacts associated with plant water stress [1,2]. For instance, Cui et al. [3] emphasized that water stress leads to a reduction in yield, as their findings indicate that water deficits disrupt the vegetative cycle, ultimately resulting in decreased productivity. While research underscores the disastrous consequences of insufficient water, it is also important to recognize that excessive use of water can adversely affect plant growth and productivity. In China, especially the North China Plain (NCP) stands as the predominant wheat cultivation region in China, contributing approximately 40-60% of the nation's overall wheat production [4]. Research conducted by Wang et al. [5] highlights significant issues related to water scarcity and the over-extraction of groundwater in the NCP, which have garnered international attention. Given the critical role of wheat as a staple food in this area, effective irrigation practices are essential for optimizing crop yields. This situation requires the implementing of monitoring methods to detect wheat water stress. One such method involves estimating the water content of plants, such as through the use of Plant Water Content (PWC) assessments.

Plant water content (PWC), a critical monitoring indicator of crop water status, plays a reference role in irrigation management [6]. There are two main indicators for PWC: the gravimetric water content (GWC, %) and the equivalent water thickness (EWT, g cm−2). Gravimetric water content (GWC) is a relative indicator for Plant water content (PWC) and does not include the effect of leaf area index and specific leaf weight [7]. The GWC of the vegetation is taken as the indicator of PWC in this study. Traditional methods for estimating plant water content have primarily been employed to monitor plant water stress. The measurement of PWC can be carried out in the field for each plant using ground-based measurements, which are time-consuming and do not reflect the spatial variability of water status in the whole field condition. In an effort to address these limitations, researchers have developed alternative techniques for monitoring plant water stress content. These techniques include the use of remote sensing imaging tools such satellite, airborne, and unmanned aerial vehicles (UAVs) platforms. For instance, remote sensing platforms have been used to assess the spatial variability of water status in larger areas [8]. Remote sensing platform offer alternative non-destructive method to field sampling and provide continuous spatial coverage over a large area. Such innovative methods have facilitated the acquisition of real-time data for tracking plant water stress. Nonetheless, the satellite and aircraft platforms present a range of challenges, such as high operational costs for data collection via aircraft and resolution issues with satellite images [9]. Both platforms may also encounter problems related to cloud cover, which can hinder data collection efforts. These challenges associated with satellite and aircraft platforms have prompted researchers to explore UAV as viable alternative, given their lower operational costs, high resolution, and ability to fly at altitudes below cloud cover [1]. The advancement of UAV technology is providing a new avenue with high-resolution mapping for accurate measurements of various spectral indexes using multispectral, thermal, and hyperspectral sensors. UAV platform has the potential to carry multispectral, hyperspectral, and thermal sensors to provide high-resolution images [10,11] and can be used to assess crop biophysical parameters [12,13]. Spectral indices information derived from these sensors can predict several physiological variables, specifically the spatial variability of plant water content [14]. Traditionally, most studies retrieve plant water status from the Near-infrared and the because of the water absorption in these bands [15]. However, some researchers have suggested that several indices using information from the electromagnetic spectrum (500-800 nm) can estimate crop water status indirectly [16,17]. Besides, high-resolution thermal imagery acquired by a UAV was successfully used to map wheat plant water stress and its spatial variability [18]. Multispectral cameras have absorption zones between 500 and 800 nm, which poses a problem when using these cameras to estimate PWC. However, the development of machine learning algorithms has provided powerful nonlinear problems solving tools and modeling techniques that can be used to estimate the PWC [19]. Past studies have shown that biochemical components have an indirect relationship with PWC. The quantity of green, blue, and red received by the plants indirectly informs the content of water molecules retained by plants.

Recently, the field of agriculture has seen a growing interest among researchers in machine learning (ML) techniques, primarily due to their superior processing speed when compared to traditional linear regression methods [18,20,21]. The advantage of this approach is the low cost of the UAV platform and payload sensors can be used to estimate the PWC of the crop wheat. Artificial neural networks (ANN) and deep neural networks (DNN) are machine learning techniques used in many research areas (engineering, agriculture, etc.) and have yielded very good results [22,23]. However, the DNN is a new branch in ML which allows more layers in the hidden layers. Due to these advantages of ML, it was reported that the DNN method can accurately predict fruit water status spatial variability [3] and plant chlorophyll content [1]. For instance, Sahoo et al. [23] explored the utilization of ML and UAVs for the purpose of mapping experimental wheat crop fields. The results of their research demonstrated that the integration of remote sensing measurements obtained from UAV imaging platforms with ML techniques is highly effective and proficient in accurately assessing the biological parameters of wheat. In this study, ANN and DNN models were used for modeling the PWC using multispectral and thermal data. A statistical comparison has been conducted between measured data and predicted data with ANN and DNN models. This study aims to develop and validate ANN and DNN algorithms to predict PWC from the multispectral and thermal images using a UAV imaging platform.

2. Material and methods

2.1. Experiment site and design

The study area is located in the north China plain (NCP), the Farmland Irrigation Research Institute experimental site in Xinxiang (Latitude: 35.15°, Longitude: 113.79°). Three (one rainout shelter experiment and two rainfed field) experiments were conducted. The area experiences a temperate continental climate characterized by an average yearly temperature ranging from approximately 4 to 13 °C. Additionally, the mean annual precipitation varies between about 300 and 800 mm, with the majority of rainfall occurring in the months of July and August (Zhang et al. [24]. The soil information of the study area are available in Zain et al. [25] . The wheat experiment was carried out from October to May 2019. There were two main blocks in the two rainout shelter experiments (Exp. 1). The first block consists of four water levels (0, 120, 240, and 360 mm) × one low nitrogen treatment (75 N t. ha^{-1}), and the second block includes the same four water levels × one high nitrogen treatment (225 N t. ha^{-1}). The other two rainfed experiments were the same water levels with different nitrogen treatments. Treatments were assigned to plots following a completely randomized block design. Nitrogen fertilizer is applied in the form of granular (urea) in the three experiments.

2.2. Unmanned aerial vehicle flyover and data collection and processing

The research utilized a multi-rotor UAV of the Spreading Wings model, equipped with sophisticated flight control capabilities that incorporate internal sensors for enhanced stability and GPS navigation. The UAV is outfitted with thermal and multispectral cameras positioned beneath its frame. Among the multispectral options, the MAPIR Survey 3 is notable for its three spectral bands: red, green, and near-infrared (NIR). This device is capable of capturing images across these three bands simultaneously, utilizing an external USB GPS receiver to ensure precise timing, with a resolution of 4000 × 3000 pixels for the red (660 nm), green (550 nm), and NIR (850 nm) bands. Following the acquisition of multispectral and thermal imagery, the Pix4D Mapper software (Pix4D S.A., Lausanne, Switzerland) was employed for image mosaicking and radiometric calibration. Once these processes were finalized, vegetation and thermal indices were computed using the raster calculator function available in ArcMap 10.3 software.

2.3. Measurements of PWC content

The assessment of above-ground fresh matter (FM) and dry matter (DM) involved the collection of plant samples from an area measuring 0.36 m^2 within each plot, which were subjected to destructive analysis throughout the growth period of the crops. These samples were subsequently transported to the laboratory for the purpose of measuring their water content. In the laboratory, the leaves collected from the designated sampling area were carefully separated from their respective stems. The fresh weights of both the leaves and stems were recorded using a precision laboratory analytical scale. Following this, the fresh samples were subjected to drying in an oven at a temperature of 75 °C until a stable dry weight was achieved. The plant water content (PWC) for all leaves and stems within the sampled area was determined as follows:

$$PWC=100\%\times((FM-DM))\ /FM \quad \ldots\ldots\ldots\ldots\ldots\ldots(1)$$

Vegetation and thermal indices model inputs

The choice of three VIs such as the Normalized Difference Vegetation Index (NDVI), the Green Normalized Difference Vegetation Index (GNDVI) and the Optimized Soil-Adjusted Vegetation Index (OSAVI) was guided by their established correlations with various biophysical traits of plants, including chlorophyll, water, and nitrogen levels. These three VIs may facilitate the indirect assessment of Plant Water Content (PWC) by analyzing the biochemical components of wheat plants. Poblete et al. [19] successfully utilized VIs such as NDVI and OSAVI to investigate the spatial variability of water status in grapevines through artificial neural network methodologies. Similarly, Carlos et al. [26]examined water stress in subsurface irrigated grapevines by employing GNDVI, NDVI, and canopy temperature measurements. Moreover, a multitude of studies have integrated the Crop Water Stress Index (CWSI) to assess plant water stress [27,28], and the positive results obtained from these indices have prompted their incorporation as variables in our regression analyses. The thermal index was chosen based on its prior use in identifying water stress in plants, with the connection between surface temperature and water stress based on crop transpiration principles. Specifically, during transpiration, the resulting evaporative cooling causes leaf temperatures to drop below that of the ambient air; in contrast, a decrease in transpiration due to water stress results in elevated leaf temperatures. The incorporation of CWSI into machine learning (ML) models may further enhance the precise evaluation of PWC within both artificial neural networks (ANN) and deep neural networks (DNN).

2.4. Regression models with UAV multispectral and thermal indices

Table 1 shows the statistical description of the dataset. Six (6) flights were conducted, and the stem elongation (SE) and grain filling stages data were used for the model's training, cross-validation, and testing. The dependent variable is represented by PWC data, whereas the independent variables include NDVI, GNDVI, OSAVI, and CWSI. For the purpose of the regression model, 70% of the data was utilized for training. The remaining 30% of the data was divided equally between the cross-validation stage and the testing stage, each comprising 15%.

Table 1 The statistical description of the dataset used for plant water content (PWC) assessment

	Min	**Max**	**Mean**	**Std. Dev.**
Input				
NDVI	0.50	0.73	0.66	± 0.06
GNDVI	0.58	0.89	0.75	± 0.08
OSAVI	0.49	0.70	0.64	± 0.06
CWSI	-0.15	1.18	0.39	± 0.25
Target				
PWC	53.00	90.72	71.57	± 9.12

2.5. ANN and DNN development

The architecture of the neural network comprises an input layer, one or more hidden layers, and an output layer. The Feed Forward Back Propagation algorithm was implemented using MATLAB software to predict the PWC. Within the network model, the choice of activation functions plays a vital role in enhancing the accuracy of the outputs and ensuring the computational efficiency during the training phase. This research explores various network configurations, alongside a range of activation functions and training algorithms. For ANN, several activation functions were employed, including the Linear Function (purelin), Sigmoid logistic (Logsig), and Sigmoid tangent (Tansig). Additionally, advanced activation functions such as Rectified Linear Unit (ReLU), Leaky Rectified Linear Unit (LeakyReLU), and Exponential Linear Unit (EluReLU) were considered within the context of DNN. The selection of these functions is critical for optimizing the performance and learning capabilities of the model.

2.6. Decision tree

In addition, a decision tree algorithm was employed to analyze input parameters such as NDVI, GNDVI, OSAVI, and CSWI, in order to assess their significance in enhancing the performance of ANN and DNN. The decision tree serves as a versatile algorithm applicable to both regression and classification tasks. Beyond its primary functions, it is also instrumental in extracting the importance of input features during the modeling process involving intelligent models. One of the key objectives of utilizing this algorithm is to elucidate the weights of input variables in relation to the output variable. Understanding the influence of each variable aids researchers in selecting those that have a substantial impact on the output variable.

2.7. Linear Regression model

Linear regression $y = \alpha x + b$ is used to evaluate each VI with PWC, where y is the dependent variable, x is the independent variable (predictors), b is the intercept, and α is the slope. Additionally, a stepwise regression model (SRM) is used to predict PWC using VIs. It is an alternative variable selection method that has been developed to identify good subset models, with considerably less computing than is required for all possible regressions. The subset models are identified the number of subsets of variables sequentially by adding or deleting, depending on the method, the one variable that has the greatest impact on the residual sum of squares.

2.8. Data pre-processing phase

In the present research, normalization of the input variables was employed to prevent data saturation, as noted. The primary aim of this normalization process is to adjust the features of the input variables so that they are comparable and fall within a uniform scale, specifically within the interval (0, 1).

2.9. Model performance statistical metrics

Several statistical metrics to assess the performance of the models, specifically the coefficient of determination (R^2), the Nash-Sutcliffe efficiency coefficient (ENS), the root mean square error (RMSE), and the mean absolute error (MAE). The coefficient of determination (R^2) quantifies the correlation between the observed and predicted data points. Additionally, the Nash-Sutcliffe efficiency (ENS), a metric established by Nash and Sutcliffe in 1970, is recognized as a prominent criterion for evaluating model efficacy. The RMSE serves as an indicator of the model's goodness of fit, particularly relevant for high flow scenarios, while the MAE provides a measure of the average error magnitude between observed and predicted values, disregarding the direction of the errors.

3. Results

3.1. Linear regression model performance evaluation

The relationship between the canopy spectral indices of wheat plants, specifically NDVI, GNDVI, OSAVI, and CWSI and PWC is illustrated in Figure 1. Among these indices, GNDVI exhibited the strongest coefficient of determination (R^2) with PWC, while NDVI, OSAVI, and CWSI demonstrated weaker correlations. Notably, CWSI displayed a negative correlation with PWC, indicating that as the values of the vegetation indices increase, PWC also tends to rise, whereas a decrease in CWSI corresponds to an increase in PWC. To further explore the linear associations between PWC and the four vegetation indices, a stepwise regression model (SRM) was employed. The statistical metrics, including R^2, ENS, RMSE, and MAE, for the training, cross-validation, and testing phases are summarized in Table 2, which details the SRM's predictive performance regarding PWC. During the training phase, the SRM achieved R^2 and ENS values of 0.75, with RMSE and MAE recorded at 1.67% and 1.37%, respectively. In contrast, the testing phase yielded R^2 and ENS values of 0.70 and 0.70, indicating a decline in model performance compared to the training stage. The findings suggest that the SRM outperformed individual vegetation indices in terms of R^2 value. Furthermore, the analysis revealed that only NDVI, GNDVI, and OSAVI were incorporated into the SRM, while CWSI was excluded from the model. The comprehensive statistical parameters of the SRM are presented in Table 3, providing a detailed overview of the model's efficacy in predicting PWC. The expression for the SRM (y) is as follows:

$$y = -10.71 + 109.48 \times NDVI + 2.83 \times GNDVI - 119.87 \times OSAVI - 233 \times \text{NDVI} \times \text{GNDVI} + 252.92 \times \text{GNDVI} \times \text{OSAVI} \quad \ldots\ldots\ldots\ldots (2)$$

Table 2 Optimum stepwise regression model (SRM) during the training, validation, and testing stages

	Training				**Cross-validation**				**Testing**			
	R^2	**E_{NS}**	**RMSE (%)**	**MAE (%)**	**R^2**	**E_{NS}**	**RMSE (%)**	**MAE (%)**	**R^2**	**E_{NS}**	**RMSE (%)**	**MAE (%)**
SRM	0.75	0.751	1.67	1.36	0.67	0.65	1.76	1.50	0.70	0.70	1.92	1.40

Table 3 Statistical performance parameters of the stepwise regression model (SRM)

	Estimate	**SE**	**t-Stat**	**pValue**
(Intercept)	-0.10717	0.15845	-0.67633	0.50044
NDVI	109.48	45.153	2.4245	0.01718
GNDVI	2.8336	1.3891	2.0399	0.044082
OSAVI	-119.87	53.496	-2.2408	0.02732
NDVI × GNDVI	-233.52	36.89	-6.3301	$7.61E^{-09}$
GNDVI ×OSAVI	252.92	36.941	6.8466	$6.89E^{-10}$

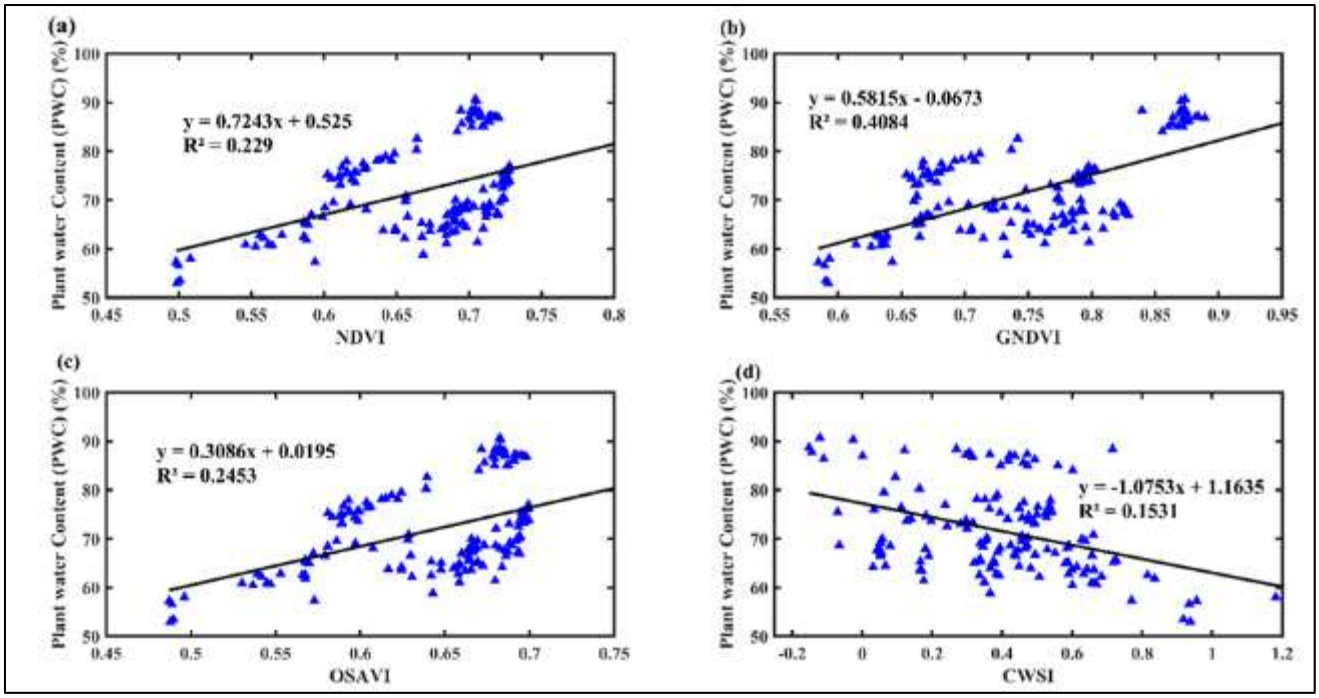

Figure 1 The relationships between different VIs, TI, and PWC (a: NDVI; b: OSAVI; c: GNDVI; d: CWSI)

The outcomes derived from the application of the decision algorithm are illustrated in Figure 1. The various input variables, each accompanied by a percentage that reflects their significance in influencing PWC. The data presented in Figure 2 indicates that the GNVI holds a substantial importance level of 68%, surpassing that of the NDVI, while the OSAVI CWSI exhibit the least significance, both at 7%. Furthermore, analyses conducted through linear regression, the SRM, and decision tree algorithms confirm that GNVI serves as the most effective input parameter for predicting PWC.

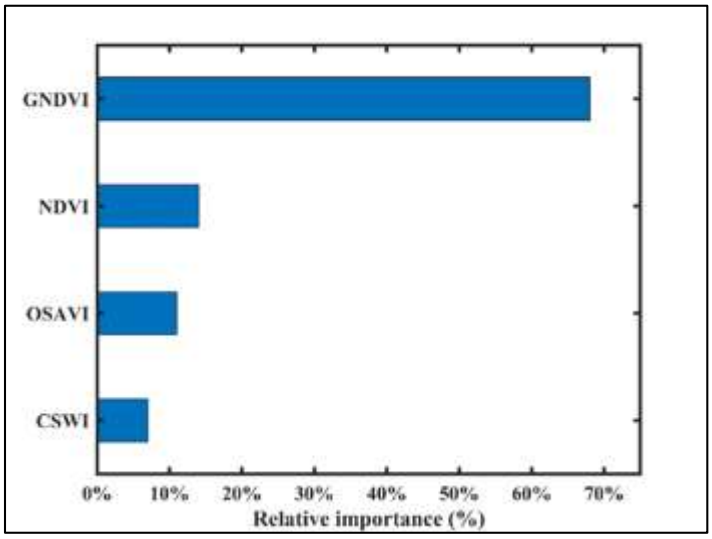

Figure 2 Input variables with their relative importance in ANN and DNN models

3.2. ANN and DNN Algorithms Performances Evaluation

A feedforward backpropagation algorithm employing various artificial neural networks (ANN) and deep neural networks (DNN) has been implemented for a regression model, utilizing different vegetation indices (VIs) such as NDVI, OSAVI, and GNDVI, along with the CWSI as inputs to predict plant water content (PWC) as the target variable. The dataset comprised 147 samples, with 70% allocated for training the network, while 15% was designated for validation and the remaining 15% for cross-validation across both ANN and DNN frameworks. To ensure effective training of the network, the input data underwent normalization. The learning algorithm for the ANN was based on Batch Gradient

Descent with Momentum, utilizing a learning rate and momentum coefficient of 0.2, with the activation functions being the hyperbolic tangent and logistic sigmoid for the input and hidden layers, respectively, while a linear function was employed in the output layer. Conversely, the DNN model utilized the Adam optimizer with a learning rate of 0.001, incorporating Relu, Leakyrelu, and Elu as transfer functions in the input and hidden layers, and a regression layer in the output. The optimal configurations for both ANN and DNN were identified by evaluating various hidden layer counts and neuron quantities within those layers, with the most effective structures being those that exhibited the lowest RMSE and MAE, alongside the highest coefficients of determination R^2 and ENS. Tables 4 and 9 detail the performance metrics, including R^2, ENS, RMSE, and MAE for the different ANN and DNN architectures. As indicated in Table 4, the most effective ANN structure for modeling PWC, when utilizing VIs and CWSI as inputs, consisted of two hidden layers. In contrast, the DNN model demonstrated optimal performance with configurations that included at least three hidden layers, as shown in Table 5.

Table 4 Optimum model of ANN structures during the training, validation, and testing stages

Model	Optimum network	Transfer functions	Training				Cross-validation				Testing			
			R^2	E_{NS}	RMSE (%)	MAE (%)	R^2	E_{NS}	RMSE (%)	MAE (%)	R^2	E_{NS}	RMSE (%)	MAE (%)
1	4-10-4-1	{tansig, tansig, linear}	0.91	0.91	2.42	1.85	0.94	0.94	2.58	2.01	0.92	0.89	2.95	2.35
2	4-10-4-1	{tansig, logsig, linear}	0.95	0.95	1.99	1.55	0.95	0.94	2.06	1.68	0.93	0.89	2.89	2.53
3	4-10-2-1	{tansig, tansig, linear}	0.94	0.94	2.12	1.63	0.96	0.95	2.44	1.78	0.95	1.86	0.95	1.50
4	4-8-1	{tansig, linear}	0.92	0.92	2.48	1.96	0.94	0.93	2.20	1.69	0.90	0.88	3.38	2.44
5	4-10-4-1	{logsig,logsig, linear}	0.85	0.85	3.24	2.60	0.81	0.80	3.90	2.83	0.88	0.87	3.78	2.90
6	4-10-2-1	{logsig,tansig, linear}	0.79	0.79	4.04	3.28	0.80	0.78	4.27	3.12	0.79	0.78	3.97	3.12
7	4-10-10-1	{tansig, logsig, linear}	0.95	0.95	1.72	1.39	0.95	0.95	2.20	1.51	0.95	0.95	2.25	1.73
8	4-10-10-1	{tansig, tansig, linear}	0.94	0.94	1.99	1.55	0.97	0.97	1.69	1.25	0.95	0.94	2.24	1.93

3.3. Comparison of Predictive Accuracy of ANN and DNN structure

The performance of ANN and DNN models was good for the training, cross-validation, and testing periods for the majority of the optimum network (Tables 4 and 5). To assess PWC, model 7 from the ANN structures and model 7 from DNN which had the highest level of accuracies were used. The scatter plots of predicted values from ANN (model 7) and DNN (model 7) models and the observed values were statistically satisfactory. As it was shown in Figure 3, during the testing periods, the R^2 regression for ANN and DNN models were respectively 0.9487 and 0.9549, However, the performance DNN network was found to be better for the ANN network during training and validation. According to the three parameters for assessing the performance of the ANN and DNN models, the best structure should have the lowest RMSE and MAE, and the value of R^2 and ENS close to 1. Table 6, by considering all the data set, shows the statistical indices comparing the ANN and DNN models used to assess PWC. The computational performance observed with the DNN models was higher than that with ANN models. The performance accuracies of PWC modeled using the ANN algorithms were in the range of 0.79-0.95 (R^2), 0.79-0.95 (E_{NS}), 1.89-4.07% (RMSE), and 3.23- 1.46% (MAE). While for DNN, they were in the range of 0.93- 0.98 (R^2), 0.93-0.98 (E_{NS}), 1.4-2.39% (RMSE) and 1.83-0.98% (MAE). It was observed that the accuracies of the models varied according to the typology of the network and the transfer functions. The DNN (model 7) was found to be the best algorithm, statistically, for modeling PWC using vegetation indices (VIs) and CWSI. In this study, it had the highest accuracy indices (R^2=0.98, E_{NS}= 0.98, RMSE= 1.37%, MAE= 0.98%.). Of the neural networks, the ANN model (6) produced the weakest model. A cross-comparison of all the employed models showed that in terms of performance, they ranked in order of DNN and ANN, except for DNN (models 6,3, and 2). These results clearly showed that the DNN models are very effective for predicting PWC when compared to ANN models.

Multilayered deep architecture is one of the characteristics of DNN and some studies found relations between the depth of the model and the predictive accuracy of the model. As seen in Table 6, the best DNN structure is composed of four hidden layers and in each hidden layer, there were twenty neurons. By using the Adam training algorithm, the optimal DNN model 7 (4-20-20-20-20-1) produced a signal in the hidden layers through the ReLU transfer function and the last layer output neuron received the combined from the last hidden layer and translate these signals into prediction using the linear function. However, the optimal network architecture for the ANN model was obtained when the network had two hidden layers, the first hidden layer had ten neurons and had activation of the sigmoid tangent transfer function and the second layer had also 10 neurons and activation of the sigmoid logistic function and the output layer of the linear transfer function (model 7). The R^2 for the optimal structure network model 7 was 0.95; E_{NS} was 0.95, RMSE was 1.89% and MAE was 1.46%. Figure 4 used the two best structures of ANN and DNN models and the results show that the predicted PWC matched the measured PWC derived from the Lab measurement for both ANN and DNN models.

Table 5 The optimum network of DNN using the Adam optimizer algorithm during the training, validation, and testing stages

Model	Optimum network	Transfer functions	Training				Cross-validation				Testing			
			R^2	E_{NS}	RMSE (%)	MAE (%)	R^2	E_{NS}	RMSE (%)	MAE (%)	R^2	E_{NS}	RMSE (%)	MAE (%)
1	4-10-10-10-1	ReLU	0.96	0.96	1.70	1.33	0.96	0.96	1.90	1.41	0.95	0.94	2.22	0.96
2	4-10-10-10-1	leakyReLU	0.93	0.93	2.37	1.82	0.92	0.90	2.29	1.70	0.93	0.93	2.53	0.93
3	4-10-10-10-1	eluReLU	0.93	0.93	2.32	1.81	0.92	0.91	2.85	0.95	0.95	1.83	0.95	0.93
4	4-10-20-20-10-1	ReLU	0.97	0.97	1.48	1.18	0.96	0.96	1.49	1.26	0.94	0.94	2.38	0.97
5	4-10-20-20-10-1	leakyReLU	0.96	0.96	1.74	1.34	0.93	0.92	2.35	1.94	0.95	0.94	1.52	0.96
6	4-10-20-20-10-1	eluReLU	0.94	0.94	2.14	1.70	0.96	0.96	1.86	1.64	0.92	0.92	2.32	0.94
7	4-20-20-20-20-1	ReLU	0.99	0.99	0.97	0.72	0.96	0.95	2.21	1.72	0.95	0.94	1.80	0.99
8	4-20-20-20-20-1	leakyReLU	0.97	0.97	1.56	1.16	0.92	0.92	2.36	1.83	0.94	0.94	1.81	0.97
9	4-20-20-20-20-1	eluReLU	0.97	0.97	1.56	1.20	0.96	0.96	1.69	1.42	0.96	0.96	1.99	0.97

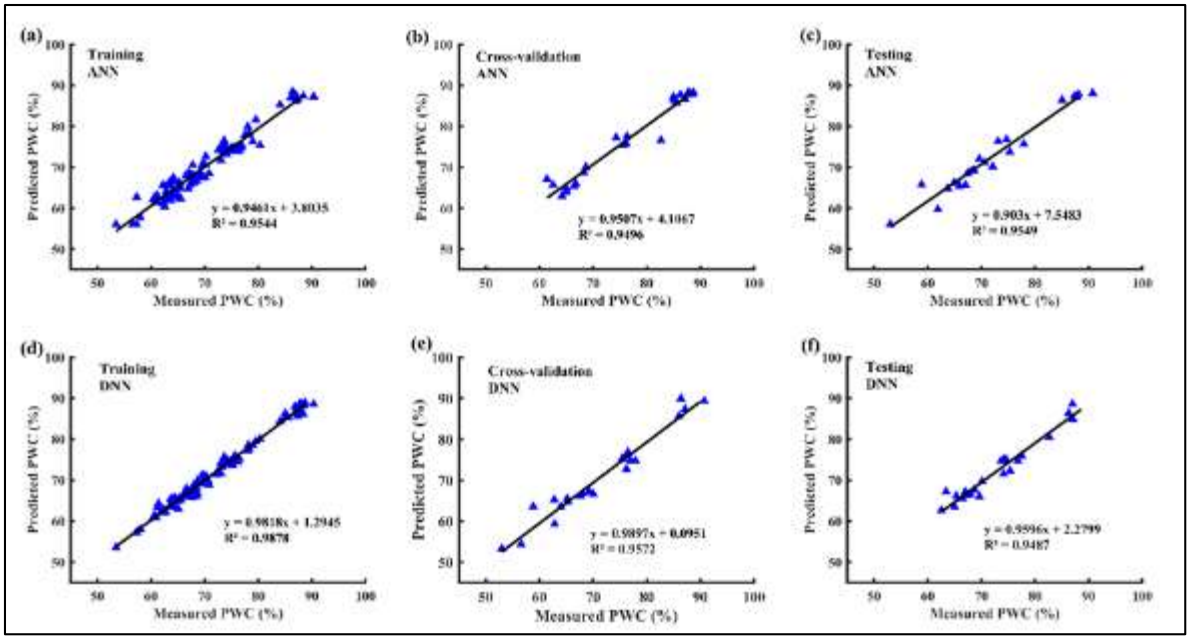

Figure 3 Measured versus predicted PWC using different network structures (a, b, and c: ANN model 7; c, d, and f: DNN model 7) during the training, cross-validation, and testing stages

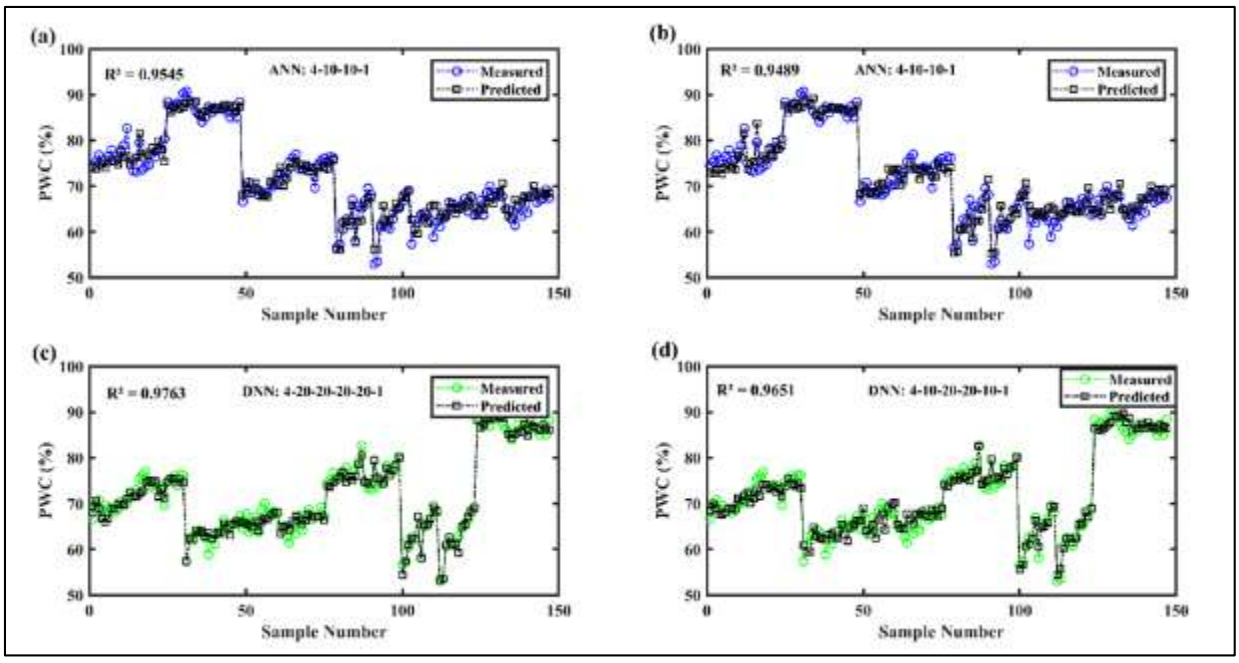

Figure 4 Comparison and relationships between measured and predicted PWC using different network structures (a: ANN model 7, b: ANN model 8; c: DNN model 7, d: DNN model 4)

3.4. ANN and DNN performance evaluation across the growth stage

Before an ANN and a DNN model can be used to assess PWC, it is important to validate the model by checking their performance in each stage. Figure 5 illustrates the prediction capability of the ANN (model 7) and DNN (model 7), the y-axis is the predicted PWC, and the x-axis represents measured PWC. The results of this study indicated that the ANN model (model 7) explained 89%, 86%, and 95% of wheat variability at stem elongation (SE), grain filling stage (GF), and across growth stages (ALL), respectively. The DNN model performed best, explaining 95%, 92%, and 98% of PWC

variability at the SE, GF, and across growth stages, respectively. A comparison between ANN and DNN showed that DNN performed better than the ANN model.

Table 6 Comparative performances statistics of the ANN and DNN models used in this study

Performance Rank	Neural Network	Model	R^2	E_{NS}	RMSE (%)	MAE (%)
1	DNN	7	0.98	0.98	1.37	0.98
2	DNN	4	0.97	0.97	1.65	1.28
3	DNN	9	0.96	0.96	1.65	1.31
4	DNN	8	0.96	0.96	1.74	1.30
5	DNN	5	0.96	0.96	1.81	1.41
6	DNN	1	0.96	0.96	1.82	1.42
7	ANN	7	0.95	0.95	1.88	1.46
8	ANN	8	0.95	0.95	1.99	1.56
9	DNN	6	0.94	0.94	2.13	1.70
10	ANN	3	0.94	0.94	2.13	1.63
11	ANN	2	0.94	0.94	2.16	1.72
12	DNN	3	0.93	0.93	2.34	1.85
13	DNN	2	0.93	0.93	2.39	1.83
14	ANN	1	0.92	0.92	2.53	1.95
15	ANN	4	0.91	0.91	2.60	1.99
16	ANN	5	0.85	0.85	3.43	2.68
17	ANN	6	0.79	0.79	4.07	3.23
18	SRM		0.67	0.51	10.79	9.03

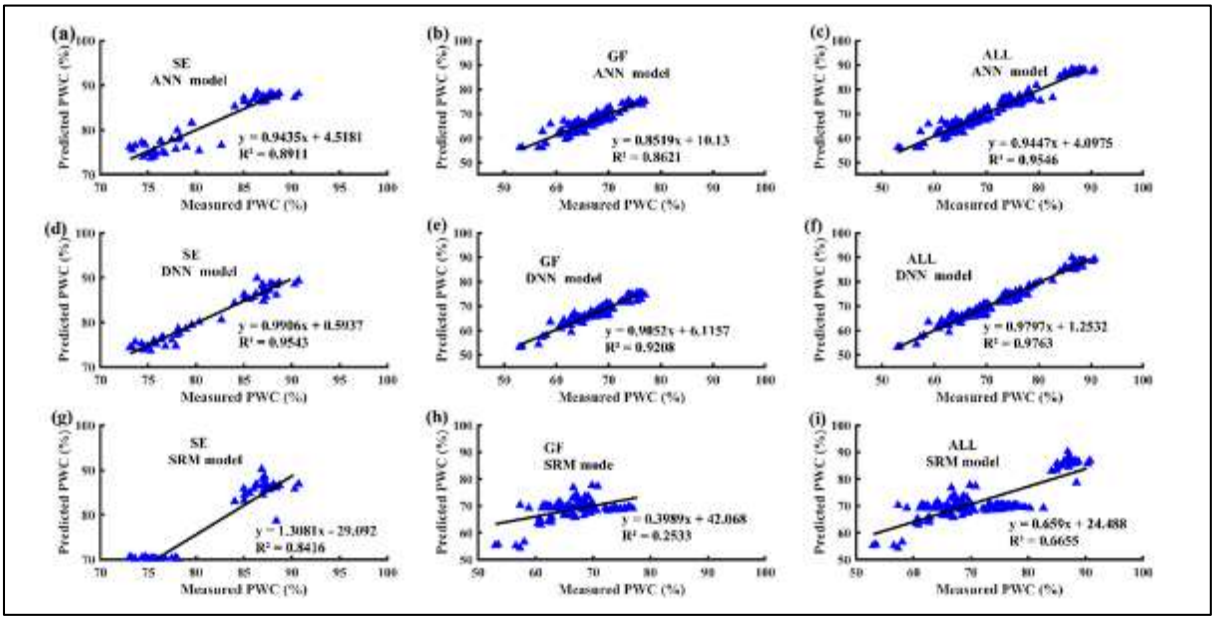

Figure 5 Relationships between predicted and observed PWC using ANN model 7(a b, and c), DNN model 7 (d, e, and f), and SMR model (g, h, and i) dataset at stem elongation (SE), grain filling (GF), and across all growth stages (ALL)

3.5. Plant water content modeling

The PWC diagnosis maps in experiment 2 were created based on the predicted PWC using the UAV remote sensing images and the ANN and DNN best models at the grain filling stage. As shown in Figure 6, the predicted PWC maps for both ANN and DNN show a visual good agreement with the RGB map and NDVI maps. The following visual comments can be drawn from the imagery in Figure 6. The soil and sampling areas where inside the fields have no vegetation cover and the model successfully assigned a low water content to areas. However, in plots 1 and 2, the DNN models give higher values of PWC to the sampling areas which are supposed to have lower water content while the ANN model successfully recognized the soils from the vegetations. The areas (Plots 7,8,9 and 10) where the growth was vigorous have higher PWC, and the best two models (ANN and DNN) successfully estimate PWC in these areas. In the areas, the nitrogen supply was higher than in plots 1 and plot 2 and the plants can accumulate more nutrients and have more capacity to maintain more water molecules. The plots receiving less than 100 kg/ha of nitrogen as classified as low PWC content (plots 1 and 2), plots receiving 100 kg/ha have medium water content (plots 4 and 5), and most plots receiving more than or equal to150 kg/ha have classified as optimal water content (plots 6, 7,8,9 and 10). The use of multispectral images, combined with thermal data can indirectly assess PWC because of the relationship between plant biomolecule and PWC. The VIs derived from multispectral images were initially designed to assess plant nitrogen content, and chlorophyll content has successfully proven to assess PWC with an RMSE varying to 1.8820, and 1.3689 for ANN and DNN models, respectively.

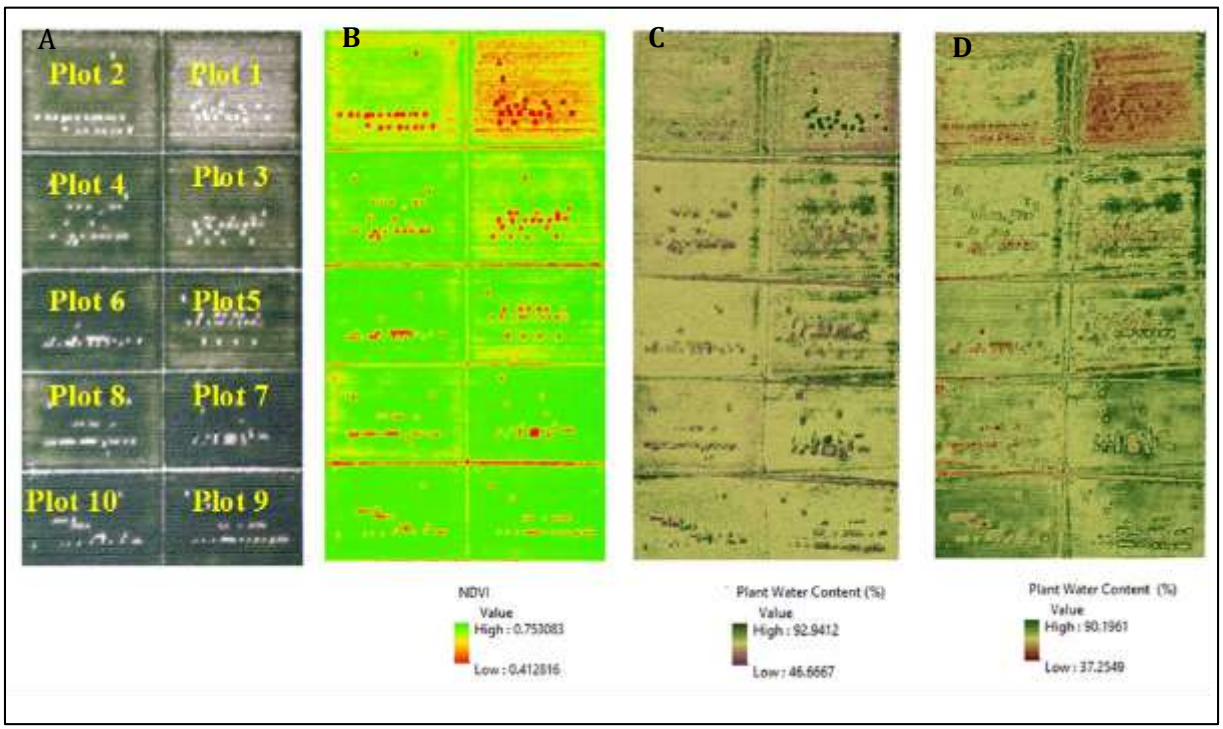

Figure 6 A RGB map, B: normalized difference vegetation index (NDVI) map, C: predicted Plant water content (PWC) map for DNN model (%), D: predicted PWC map for the ANN model (%) for the dates representing early grow filling stage in experiment 2

4. Discussion

4.1. Estimating PWC using linear regression, vegetation indices and CWSI

The application of Vegetation Indices (VIs) in this study was predicated on the understanding that the various bands employed to compute these indices were primarily selected to estimate crop bio parameters, such as chlorophyll and nitrogen content. Notably, chlorophyll is as indirect indicator for assessing the water content in plants. Our findings indicate that the Green Normalized Difference Vegetation Index (GNDVI) emerges as the most suitable VI-based estimator of Plant Water Content (PWC). The inclusion of the green band in this index may enhance the likelihood of accurately detecting chlorophyll pigments, which are indirectly associated with water presence. In contrast, the Normalized Difference Vegetation Index (NDVI) produced estimates that were not significantly different from those generated by the Optimized Soil-Adjusted Vegetation Index (OSAVI). However, NDVI, which substitutes the green band

for the red band, is susceptible to vegetation fraction issues that can compromise the effectiveness of chlorophyll absorption. Similarly, OSAVI remains sensitive to the reflectance properties of the underlying soil, as the canopy reflectance captured by UAVs results from a complex interplay of chlorophyll, canopy structure, and soil contributions. In the areas partially vegetated that generate high reflectance values can produce errors when assessing the crop parameters, researchers introduce OSAVI which takes account of the variability due to soil reflectance [29]. Furthermore, vegetation indices that are less affected by soil optical properties tend to show limited sensitivity to variations in chlorophyll levels. The correlation between CWSI and PWC showed that CWSI is negatively correlated with PWC. The CWSI increase is due to the cooling effect of the canopy transpiration which consequently decreases PWC. This can be explained by water stress which leads to a reduction of water uptake by roots, decreasing PWC, and increased CWSI values. These results agree with [30] who reported the CWSI values of barley cultivars increased with increasing plant water stress levels from mild to severe stress. The results demonstrate that the three VIs and the CWSI were useful in estimating PWC.

The results indicated that estimating SMR (R^2=0.67, E_{NS}=-0.51, RMSE=10.79%, MAE=9.03%) model for the entire dataset was more robust than traditional linear regression. The estimating accuracy using SMR was generally higher than that of traditional linear regression. However, compared with ANN and DNN models, the computational performance observed with the SMR regression method was lower than that with the ANN and DNN models (Figure. 5). Liu et al. [31] found that the machine learning models such as ANN had much higher estimation accuracy than SMR.

4.2. Models' performance accuracies

ML models have been used to identify complex nonlinear relationships between input and output in several agricultural studies. ANN was first introduced as a general method to find a nonlinear relationship between input and output data. Traditionally, the ANN models used the transfer function sigmoid tangent and log sigmoid to process values passing through neurons from one layer to the next layer. The results showed that, the DNN model with relu activation layer and four hidden layers performed consistently better than the other ANN and SRM. The superior performance of DNN compared to ANN can be attributed to the inadequacy of the activation functions employed in ANN, specifically the logistic sigmoid and hyperbolic tangent functions. These functions are not well-suited for training extensive networks, primarily because they are susceptible to the vanishing gradient problem, which hampers effective learning in deeper architectures. However, our findings indicate that DNN methodologies effectively address the vanishing gradient issue, thereby enhancing predictive accuracy. There is a growing consensus that DNN architectures outperform traditional artificial neural networks (ANNs). In this research, the application of the Rectified Linear Unit (ReLU), as noted by Nair and Hinton (2010), when combined with the Adam optimization algorithm, resulted in significant improvements in the accuracy of model performance. The current study's results demonstrate a strong correlation between the models and the experimental data. Consequently, ML techniques are employed to conduct regression analyses on complex nonlinear problems, facilitating the identification of intricate relationships between various input datasets, including NDVI, GNDVI, OSAVI, and CWSI, and the output dataset, which is PWC. This approach underscores the capability of ML to unravel nonlinear dynamics within the data, further validating the efficacy of DNN models in predictive analytics.

ANN models have been used to predict other crop parameters. For instance, Poblete et al. [19] found an R^2 value of 0.56- 0.87 when predicting vine water status variability multispectral data. Liu et al. [33] predict chlorophyll using ANN, they found an R^2 value of 0.96 which is inferior to the R^2 value obtained from the DNN (0.97) obtained in this study. However, in recent studies, Cui et al. [3] carried out research focused on a prediction model utilizing deep learning techniques to assess the leave water content of fruit trees. The findings indicated that the deep learning-based models significantly surpassed traditional machine learning approaches, achieving an accuracy rate of 95% or greater. This paper proposed an ANN and DNN-based prediction model to predict PWC. This study introduced a prediction model for PWC that utilizes artificial neural networks (ANN) and deep neural networks (DNN). It represents one of the initial efforts to apply deep learning techniques for predicting PWC by leveraging multispectral and thermal indices. The results indicated that the prediction accuracy achieved with the DNN model was markedly higher than that of the ANN model. Overall, the implementation of a deep learning-based approach significantly enhanced the accuracy of PWC predictions.

4.3. Advantages and limitations of ANN and DNN models

The deployment of UAV platforms offers a dependable means for diagnosing PWC. This research demonstrated that VIs and CWSI derived from thermal imagery can effectively evaluate PWC. In the present study, VIs and CWSI were utilized to generate distribution maps of wheat PWC during the seedling and grain filling growth stages, ANN and DNN for predictive modeling. These PWC maps serve as valuable tools for farmers, enabling them to pinpoint areas with insufficient water content. However, since the multispectral and thermal images originate from different cameras with varying resolutions, it is essential to standardize their resolutions to ensure accurate information extraction and

effective data input into the ANN and DNN models. The impact of image resolution on the quality of the PWC maps remains ambiguous. Furthermore, it is imperative to explore a diverse array of multispectral and thermal images captured under varying environmental conditions to assess how these variables influence the reflectance characteristics of each camera and the resulting prediction outcomes. While ANN and DNN offer certain benefits, they also come with a range of disadvantages and constraints. Additional challenges associated with ML include the difficulty in assessing the individual contribution of each input variable and the risk of overfitting, which can impair model performance when applied to new datasets. In contrast, decision tree algorithms can assign relative importance to each input variable, thereby addressing some of these concerns. Furthermore, the issue of overfitting can be mitigated by partitioning the dataset into training and validation sets, as well as by constraining the number of hidden nodes within the hidden layers.

5. Conclusion

In this research, various vegetation indices (VIs), including NDVI, GNDVI, OSAVI, and the thermal index of CWSI, demonstrated sensitivity to plant water content (PWC), leading to their selection for PWC estimation. To model PWC, artificial neural networks (ANN), deep neural networks (DNN), and linear regression models were employed, utilizing multispectral and thermal imagery. The input layers of both the ANN and DNN models comprised NDVI, GNDVI, OSAVI, and CWSI, while the output layer represented PWC. The prediction performance of both ANN and DNN models, following training and testing, was deemed satisfactory, indicating their potential applicability in modeling PWC. Notably, the DNN model outperformed the ANN model, achieving significantly higher prediction accuracy, with DNN models reaching an accuracy of 92% or more. Therefore, the DNN approach is anticipated to yield more effective predictions of PWC through the use of multispectral and thermal data. Developing a PWC assessment model utilizing UAV remote sensing data is essential, as it would improve the accuracy of PWC retrievals. The findings from such research could assist farmers in making informed irrigation decisions. With the rapid advancement of machine learning techniques and UAV platforms equipped with high-resolution imagery, these estimation models could be seamlessly integrated into agricultural management tools.

Compliance with ethical standards

Acknowledgments

This study was supported by the National Natural Science Foundation of China (51609247), the China Agriculture Research System (CARS-02, CARS-3-1-30). The authors are thankful to the Chinese Academy of agricultural science for kindly providing the equipment.

Disclosure of conflict of interest

The authors declare that they have no conflict of interest.

References

[1] Li, J.; Wijewardane, N.K.; Ge, Y.; Shi, Y. Improved Chlorophyll and Water Content Estimations at Leaf Level with a Hybrid Radiative Transfer and Machine Learning Model. Comput. Electron. Agric., 2023, 206, 107669.

[2] Liu, S.; Peng, Y.; Du, W.; Le, Y.; Li, L. Remote Estimation of Leaf and Canopy Water Content in Winter Wheat with Different Vertical Distribution of Water-Related Properties. Remote Sens., 2015, 7, 4626–4650.

[3] Cui, J.; Sawut, M.; Ailijiang, N.; Manlike, A.; Hu, X. Estimation of Leaf Water Content of a Fruit Tree by In Situ Vis-NIR Spectroscopy Using Multiple Machine Learning. 2024.

[4] Jun-Fang, Z.; Jian-Ping, G. Possible Trajectories of Agricultural Cropping Systems in China from 2011 to 2050. Am. J. Clim. Chang., 2013, 2, 191–197.

[5] Wang, X.; Li, X.; Fischer, G.; Sun, L.; Tan, M.; Xin, L.; Liang, Z. Impact of the Changing Area Sown to Winter Wheat on Crop Water Footprint in the North China Plain. Ecol. Indic., 2015, 57, 100–109.

[6] Alibabaei, K.; Gaspar, P.D.; Lima, T.M. Big Data and Irrigation Scheduling. energies, 2021, 1–21.

[7] Zhang, Z.; Tang, B.H.; Li, Z.L. Retrieval of Leaf Water Content from Remotely Sensed Data Using a Vegetation Index Model Constructed with Shortwave Infrared Reflectances. Int. J. Remote Sens., 2019, 40, 2313–2323.

[8] Parsinejad, M.; Raja, O.; Chehrenegar, B. Practical Analysis of Remote Sensing Estimations of Water Use for Major Crops throughout the Urmia Lake Basin. Agric. Water Manag., 2022, 260, 107232.

[9] Jin, X.; Li, Z.; Feng, H.; Ren, Z.; Li, S. Deep Neural Network Algorithm for Estimating Maize Biomass Based on Simulated Sentinel 2A Vegetation Indices and Leaf Area Index. Crop J., 2020, 8, 87–97.

[10] Niu, Y.; Han, W.; Zhang, H.; Zhang, L.; Chen, H. Estimating Fractional Vegetation Cover of Maize under Water Stress from UAV Multispectral Imagery Using Machine Learning Algorithms. Comput. Electron. Agric., 2021, 189, 106414.

[11] Maier, K.; Nascetti, A.; van Pelt, W.; Rosqvist, G. Direct Photogrammetry with Multispectral Imagery for UAV-Based Snow Depth Estimation. ISPRS J. Photogramm. Remote Sens., 2022, 186, 1–18.

[12] Hou, M.; Tian, F.; Ortega-Farias, S.; Riveros-Burgos, C.; Zhang, T.; Lin, A. Estimation of Crop Transpiration and Its Scale Effect Based on Ground and UAV Thermal Infrared Remote Sensing Images. Eur. J. Agron., 2021, 131, 126389.

[13] Yang, X.; Yang, R.; Ye, Y.; Yuan, Z.; Wang, D.; Hua, K. Winter Wheat SPAD Estimation from UAV Hyperspectral Data Using Cluster-Regression Methods. Int. J. Appl. Earth Obs. Geoinf., 2021, 105, 102618.

[14] Penuelas, J.; Filella, I.; Biel, C.; Serrano, L.; Savé, R. The Reflectance at the 950-970 Nm Region as an Indicator of Plant Water Staus. Int. J. Remote Sens., 1993, 14, 1887–1905.

[15] Sibanda, M.; Mutanga, O.; Dube, T.; Mothapo, M.C.; Mafongoya, P.L. Remote Sensing Equivalent Water Thickness of Grass Treated with Different Fertiliser Regimes Using Resample HyspIRI and EnMAP Data. Phys. Chem. Earth, Parts A/B/C, 2019, 112, 246–254.

[16] Penuelas, J.; Pinol, J.; Ogaya, R.; Filella, I. Estimation of Plant Water Concentration by the Reflectance Water Index WI (R900 / R970). Int. J. Remote Sens., 1997, 18, 2869–2875.

[17] Rallo, G.; Minacapilli, M.; Ciraolo, G.; Provenzano, G. Detecting Crop Water Status in Mature Olive Groves Using Vegetation Spectral Measurements. Biosyst. Eng., 2014, 128, 52–68.

[18] Wang, J.; Lou, Y.; Wang, W.; Liu, S.; Zhang, H.; Hui, X.; Wang, Y.; Yan, H.; Maes, W.H. A Robust Model for Diagnosing Water Stress of Winter Wheat by Combining UAV Multispectral and Thermal Remote Sensing. Agric. Water Manag., 2024, 291, 108616.

[19] Poblete, T.; Ortega-far, S.; Bardeen, M. Artificial Neural Network to Predict Vine Water Status Spatial Variability Using Multispectral Information Obtained from an Unmanned Aerial Vehicle (UAV). Sensors, 2017, 17.

[20] Xue, H.; Xu, X.; Zhu, Q.; Meng, Y.; Long, H.; Li, H.; Song, X.; Yang, G.; Yang, M.; Li, Y.; Jiang, X. Rice Yield and Quality Estimation Coupling Hierarchical Linear Model with Remote Sensing. Comput. Electron. Agric., 2024, 218, 108731.

[21] Ameslek, O.; Zahir, H.; Latifi, H.; Bachaoui, E.M. Combining OBIA, CNN, and UAV Imagery for Automated Detection and Mapping of Individual Olive Trees. Smart Agric. Technol., 2024, 9, 100546.

[22] De Clercq, D.; Mahdi, A. Feasibility of Machine Learning-Based Rice Yield Prediction in India at the District Level Using Climate Reanalysis and Remote Sensing Data. Agric. Syst., 2024, 220, 104099.

[23] Sahoo, R.N.; Rejith, R.G.; Gakhar, S.; Verrelst, J.; Ranjan, R.; Kondraju, T.; Meena, M.C.; Mukherjee, J.; Dass, A.; Kumar, S.; Kumar, M.; Dhandapani, R.; Chinnusamy, V. Estimation of Wheat Biophysical Variables through UAV Hyperspectral Remote Sensing Using Machine Learning and Radiative Transfer Models. Comput. Electron. Agric., 2024, 221, 108942.

[24] Zhang, H.L.; Zhao, X.; Yin, X.G.; Liu, S.L.; Xue, J.F.; Wang, M.; Pu, C.; Lal, R.; Chen, F. Challenges and Adaptations of Farming to Climate Change in the North China Plain. Clim. Change, 2015, 129, 213–224.

[25] Zain, M.; LI, S.; Gao, Y.; Mehmood, F.; Ur-rahman, S. The Coupled Effects of Irrigation Scheduling and Nitrogen Fertilization Mode on Growth, Yield and Water Use Efficiency in Drip-Irrigated Winter Wheat. Sustainability, 2021, 13, 1–18.

[26] Carlos, Z.; Khot, L.R.; Sankaran, S.; Jacoby, P.W. High Resolution Multispectral and Thermal Remote Sensing-Based Water Stress Assessment in Subsurface Irrigated Grapevines. 2017.

[27] Shaughnessy, S.A.O.; Evett, S.R.; Colaizzi, P.D.; Howell, T.A. A Crop Water Stress Index and Time Threshold for Automatic Irrigation Scheduling of Grain Sorghum. Agric. Water Manag., 2012, 107, 122–132.

[28] Jones, H.G.; Serraj, R.; Loveys, B.R.; Xiong, L.; Wheaton, A.; Price, A.H. Thermal Infrared Imaging of Crop Canopies for the Remote Diagnosis and Quanti Fi Cation of Plant Responses to Water Stress in the Fi Eld. Funct. Plant Biol., 2009, 978–989.

[29] Fern, R.R.; Foxley, E.A.; Bruno, A.; Morrison, M.L. Suitability of NDVI and OSAVI as Estimators of Green Biomass and Coverage in a Semi-Arid Rangeland. Ecol. Indic., 2018, 94, 16–21.

[30] Elsayed, S.; Elhoweity, M.; Ibrahim, H.H.; Hassan, Y.; Migdadi, H.M.; Schmidhalter, U. Thermal Imaging and Passive Reflectance Sensing to Estimate the Water Status and Grain Yield of Wheat under Different Irrigation Regimes. Agric. Water Manag., 2017, 189, 98–110.

[31] Liu, P.; Shi, R.; Gao, W. Estimating Leaf Chlorophyll Contents by Combining Multiple Spectral Indices with an Artificial Neural Network. Earth Sci. Informatics, 2018, 11, 147–156.

[32] Nair, V.; Hinton, G.E. Proceedings of the 27th International Confer- Ence on Machine Learning. In Rectified Linear Units Improve Restricted Boltzmann Machines; 2010; pp. 1–8.

[33] Liu, Z.; Qin, A.; Zhang, J.; Sun, J.; Ning, D.; Zhao, B.; Xiao, J.; Liu, Z.; Duan, A. Maize Yield as a Function of Water Availability across Precipitation Years in the North China Plain; 2017; Vol. 57.